Neurochemical Research (2019) 44:2482–2498
https://doi.org/10.1007/s11064-019-02865-7

ORIGINAL PAPER

Sepantronium Bromide (YM155), A Small Molecule Survivin Inhibitor, Promotes Apoptosis by Induction of Oxidative Stress, Worsens the Behavioral Deficits and Develops an Early Model of Toxic Demyelination: In Vivo and In-Silico Study

Samaneh Reiszadeh-Jahromi[1] · Mohammad-Reza Sepand[2] · Samaneh Ramezani-sefidar[3] · Mohsen Shahlaei[4] · Sajad Moradi[4] · Meysam Yazdankhah[5] · Nima Sanadgol[6]

Received: 17 May 2019 / Revised: 21 August 2019 / Accepted: 23 August 2019 / Published online: 5 September 2019

Abstract

Cuprizone (cup) model targets oligodendrocytes (OLGs) degeneration and is frequently used for the mechanistic understanding of de- and remyelination. Improperly, this classic model is time-consuming and the extent of brain lesions and behavioral deficits are changeable (both temporally and spatially) within a mouse strain. We aimed to offer an alternative, less time-consuming, and more reproducible cup model. Mice (C57BL/6) were treated with cup (400 mg kg^{-1} day^{-1}/gavage) for three consecutive weeks to induce OLGs degeneration with or without YM155 (1 mg kg^{-1} day^{-1}) to examine the effects of this molecule in cup neurotoxicity. Co-administration of cup and YM155 (cuYM) accelerated the intrinsic apoptosis of mature OLGs (MOG positive cells) through the upregulation of caspase-9 and caspase-3. In addition to the stimulation of oxidative stress via reduction of glutathione peroxidase and induction of malondialdehyde, behavioral deficits in both Open-field and Rota-rod tests were worsened by cuYM. In the cuYM group, the expression of BIRC5, BIRC4 and NAIP was reduced, but no significant changes were observed in the abundance of the other inhibitor of apoptosis proteins (cIAP1 and cIAP2) in comparison with the cup group. Moreover, in silico analysis validated that YM155 directly interrupts the binding sites of certain transcription factors, such as krüppel-like family (Klf), specificity proteins (SPs), myeloid zinc fingers (MZFs), zinc finger proteins (ZNFPs), and transcription factor activating enhancer-binding proteins (TFAPs), on the promoters of target genes. In conclusion, this modified model promotes cup-induced redox and apoptosis signaling, elevates behavioral deficits, saves time, minimizes variations, and can be employed for early evaluation of novel neuroprotective agents in oligodendropathies.

Keywords Apoptosis · Inhibitors of apoptosis proteins · Multiple sclerosis · Oligodendrocytes

Introduction

In multiple sclerosis (MS), the immune system wrongly attacks and destroys the myelin sheath. Ultimately, this process leads to the gradual destruction of nerve fibers, which

Electronic supplementary material The online version of this article (https://doi.org/10.1007/s11064-019-02865-7) contains supplementary material, which is available to authorized users.

✉ Nima Sanadgol
Sanadgol.n@gmail.com; n.sanadgol@uoz.ac.ir

[1] Department of Biology, University of Sistan and Baluchestan, Zahedan, Iran

[2] Department of Toxicology and Pharmacology, Faculty of Pharmacy, Tehran University of Medical Sciences, Tehran, Iran

[3] Department of Biology, Faculty of Basic Sciences, Razi University, Kermanshah, Iran

[4] Nano Drug Delivery Research Center, School of Pharmacy, Kermanshah University of Medical Science, Kermanshah, Iran

[5] Department of Ophthalmology, University of Pittsburgh School of Medicine, Pittsburgh, PA, USA

[6] Department of Biology, Faculty of Sciences, University of Zabol, Zabol, Iran

may entail disabilities in MS patients [1, 2]. During oligodendrocytes (OLGs) damage, the recruitment of immune cells and the secretion of pro-inflammatory mediators, reactive oxygen species (ROSs), and proteolytic enzymes cause tissue injury and axonal fibers destruction [3].

A copper chelating agent named cuprizone (bis-cyclohexanone-oxalyldihydrazone, cup) is frequently used in studying specific OLGs death and myelin loss, independent of autoimmune reaction. Cuprizone feeding affects ordinary OLGs metabolism through the disturbance of mitochondrial function, induction of oxidative stress, production of cytochrome c, and leading to OLGs apoptosis, similar to what occurs in type III MS lesions [4, 5]. As cup induced-mature OLGs apoptosis finally leads to an extensive demyelination in both white and gray matter regions this model is particularly supportive to explain basic cellular and molecular mechanisms during de- and remyelination independently of peripheral immune cells interactions.

The extent of demyelination in the cup model can fluctuate depending on cup feed quantity, the age and breed of the used animals and the duration of induction (4, 5 or 6 weeks), complicating the understanding of de- and remyelination processes [6]. Apoptosis in OLGs, like other cells, is a highly regulated process, subjecting to either activation or inhibition by a variety of chemical factors. Endogenous inhibitors of apoptosis are generally crucial to ensure cell survival by avoiding the uncontrolled activation of the caspases.

BIRCs (BIR domain containing proteins) and IAPs (inhibitors of apoptosis proteins) contain baculoviral IAP repeat (BIR) domains (a zinc finger motif) which are known for the regulation of immune signaling and caspases [7]. IAPs are suitable targets for increasing the survival rate of both glial and neuronal cells against chemical toxicants. Moreover, they are expressed in a wide range of tumor cells and have been targeted in recent randomized clinical trials [8]. Baculoviral IAP repeat-containing 5 (BIRC5/Survivin/TIAP), X-linked inhibitor of apoptosis protein (BIRC4/XIAP/MIHA), cellular IAP (cIAP) proteins 1 (cIAP-1/MIHB) and 2 (cIAP-2/MIHC), and neuronal apoptosis inhibitory protein (NAIP) are major IAP proteins expressed by central nervous system (CNS) neurons [9]. BIRC5 is a unique member of IAPs gene family, is well-known for its dual role as mitosis regulator and apoptosis inhibitor, and was recently considered as an important therapeutic target in brain glioma [10].

Interestingly, there are several clinical trials evaluating minocycline, as an anti-inflammatory and anti-apoptotic agent, in MS patients [11]. It has also been demonstrated that monitoring the expression patterns of IAPs in the immune system of MS patients can help to determine disease subtype and specify the molecular mechanisms responsible for different clinical outcomes [12]. Preventing, delaying, or reducing the grade of OLGs loss may become possible by altering IAPs expression pattern and addressing related behavioral dysfunctions [13].

The aim of present study was to check whether reduction in OLGs endogenous anti-apoptosis mechanisms could accelerate the rate of demyelination. Our previous data demonstrated that the expression of BIRC5 in OLGs dramatically reduced after a 6-week cup treatment in a time-dependent manner. It was postulated that OLGs survival rate throughout the cup regime could be minimized by YM155, a novel synthetic small molecule that suppresses transactivation of BIRC5/survivin through direct binding to its promoter.

Hence, for the first time, we investigated the role of IAPs expression pattern on the mature OLGs apoptosis in the presence of YM155 during cup-induced OLGs degeneration. The overall aim of this work was to offer an alternative, less time-consuming, more reproducible and generally superior model of OLGs death, in comparison to the classical cup model, through impeding of endogenous anti-apoptotic mechanisms via additional administration of YM155 compound (cupYM model). This model offers a good situation for testing potential therapeutics in order to inhibit demyelination or to enhance myelin repair in a longer remyelination period.

Material and Methods

Model Developing and Experimental Design

Eighty 7–8 weeks-old male C57BL/6 mice (18–20 g) were purchased from Pasteur Institute of Iran. Mice were kept under standard laboratory conditions with a 12-hour light/dark cycle at 20 ± 22 °C temperature. Water and food were available ad libitum, chow was changed and mice were weighed every other day. Ethical points observed according to the declaration of Helsinki and relevant code of ethics, regarding minimizing harms during animal experimentation. In the classical cup model, mice were fed with cup-containing food (either in pellets or in powdered chow) ad libitum, the major issue was discrepancy in myelin damage extent among the animals. It has been reported that controlled consumption of cup (via gavage) minimizes the interanimal inconsistency in myelin loss and hence reduces the number of used animals, providing a reliable model for pharmacological assessments [14]. So, in order to generate a consistent model, animals received 400 mg kg^{-1} body weight of cup (bis-cyclohexanone oxaldihydrazone; Sigma, St. Louis, MO) dissolved in 250 µL phosphate buffered saline (PBS, 7.2) via gavage at mornings for three consecutive weeks [14]. To create the modified model, cup was given orally for three weeks along with intraperitoneal (i.p.) administration of 1 mg kg^{-1} body weight YM155 (Cayman Chemical, Michigan, USA)

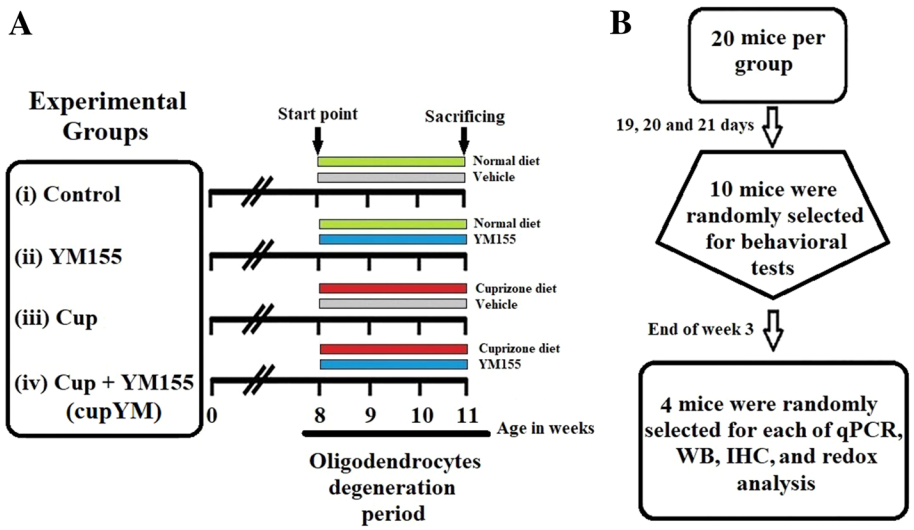

Fig. 1 Flow chart of groups design (**a**) and timelines of the experiments and number of used animals (**b**), see model developing and experimental groups section for more details

dissolved in 1:9 ratio of dimethyl sulfoxide (DMSO) and PBS (pH 7.2) in total volume of 100 µL as vehicle in specific hours at noon [15]. Mice were randomly divided into 4 major groups as graphically represented in Fig. 1 with the following specifications: (I) Control group: healthy mice fed with normal food for 3 weeks along with daily injection of vehicle (100 µL). (II) YM155 group: healthy mice fed with normal food for 3 weeks along with daily. injection of YM155 dissolved in vehicle.(III) Cuprizone (cup) group: healthy mice fed with normal food for 3 weeks along with daily gavage of cup solution along with injection of vehicle. (IV) Cup + YM155 group (cupYM): healthy mice fed with normal food for 3 weeks receiving cup in conjunction with YM155 every day. Group assignments were blinded for observer during all experimental preformation.

Sample Preparation

At the end of week 3, animals were randomly selected from every group for each test. Ten mice per group were selected for different behavioral analysis. At the end of last behavioral test in day 21, ketamine (50 mg kg^{-1}) and xylazine (4 mg kg^{-1}) were used to anesthetize animals, and mice were transcardially perfused by either PBS or paraformaldehyde (PFA) depending on the future applications. The brains of eight randomly selected mice per group were dissected on ice and the midline corpus callosum (CC) was isolated and kept at − 80 °C for the purpose of western blot (WB) analysis or quantitative polymerase chain reaction (qPCR). Moreover, the brains of four other mice per group were isolated from the skull and fixed in 4% PFA in PBS at 4 °C overnight. Subsequently, brain samples were rinsed overnight in ice-cold sucrose (30%), snap frozen, embedded in optimal cutting temperature compound (OCT, Tissue Tek) and stored in − 80 °C. Fixed brains were sectioned serially (5 µM) by the floor standing automatic cryostat (MNT-SLEE, Mainz GmbH, Germany) in the coronal planes. Sections were placed onto poly-L-lysine coated coverslips for fluorescence immunohistochemistry (FIHC) assay, where the mouse brain atlas (1.58 to 2.30 mm from the bregma) was used for midline CC identification. Remaining animals were preceded for redox analysis according to related protocols (Fig. 1).

Open-Field Test

The open-field test was performed in a standard box (50 × 50 cm with 30 cm high), where animal behavioral data (5 min) were recorded. To evaluate motor function and anxiety-like behavior, variables such as total distance (TD, cm), velocity (cm s^{-1}), duration in the central zone (DC, sec) and DC/TD ratio were calculated via video-tracking [16].

Rota-Rod Test

Motor coordination was evaluated by Rota-rod test, in which animals capability to stay on a rotating rod (rotation speed from 4 to 40 rpm) in three successive trials (2 min per trial) were measured. All groups were assessed in the afternoon of 19th, 20th and 21th day of the experiment (three times a day) with two minutes interval rest between each trial [16].

Quantitative Reverse Transcription PCR (qRT-PCR) Analysis

Extraction of total RNA, cDNA synthesis and qRT-PCR were performed as described previously [16]. Briefly, after removal of the brain, the rostral region of CC was dissected on ice, snap frozen and stored at − 80 °C for future use. RNA was extracted from 20 mg of tissue and dissolved in 50µL diethyl pyrocarbonate (DEPC) water according to the

AccuZol™ kit instructions (BIONEER, South Korea). In the next step, RNAs (5 µg per 20 µl reaction volume) were converted into cDNA using the AccuPower kit (BIONEER, South Korea). One µg of each synthesized cDNA was used for qRT-PCR assay. In each group, cDNA from four mice brain were pooled where PCR was performed in triplicates. Primer sequences and thermocycling parameters are presented as supplementary data (Supplementary Table 1). Expression values from β-actin as the reference gene were used to normalize each sample. Relative changes in expression patterns were determined using the $2^{-\Delta\Delta CT}$ methods [17].

Double-Labeling Fluorescence Immunohistochemistry (FIHC)

Immunohistochemistry was carried out according to our previous work [18]. Briefly, fixed brains were sectioned in 5 µm diameter, rehydrated and kept on H_2O_2 (0.3%) in order to block the activity of endogenous peroxidase. After washing, sections were blocked for non-specific binding with blocking solution (10% serum from host species of secondary antibody, Triton X-100 (0.05%) in PBS), and then incubated in permeabilization buffer (Triton X-100 (0.1%) in PBS). Sections were incubated overnight at 4 °C with primary antibodies against myelin oligodendrocyte glycoprotein (MOG) as the marker of mature OLGs and cleaved-caspase-3 as the marker of an end-step apoptosis. Next, samples were washed and incubated 4 h with secondary antibody diluted in antibody buffer (goat serum (5%), Triton X-100 (0.05%) in PBS). Antibodies information and dilution concentrations are presented as a supplementary data (Supplementary Table 2). Nuclei visualization, was performed by counterstaining samples with DAPI, where negative controls were obtained by omitting primary antibody with no signal (data not shown). Images were captured via digital camera under a fluorescence microscope and were analyzed by ImageJ (https://rsb.info.nih.gov/ij/) software [19]. To evaluate demyelination, sections were stained with Luxol fast blue (LFB), as described previously [20].

Western Blotting (WB) Analysis

Immunoblotting procedure was carried out as described previously [21]. Briefly, whole CC was bilaterally microdissected on ice following brain removing and quickly frozen and kept at − 80 °C until further usage. After adding complete protease inhibitor cocktail (Roche, Mannheim, Germany) tissues were homogenized and centrifuged and the protein content was measured using the bicinchoninic acid (BCA) method (Sigma-Aldrich). SDS-PAGE gel electrophoresis (8–10%) was done with equal quantities of total protein (25 µg) per lane. Resolved proteins were transferred to polyvinylidene fluoride (PVDF) membranes via electrophoretic transfer system (Bio-Rad, München, Germany). Following blocking, the membranes were incubated overnight at 4 °C with specific primary antibodies. Following membranes wash with PBS, 0.05% Tween-20 (PBS-T), all blots were incubated for 4 h at 4 °C with respective secondary antibodies. Antibodies information and dilution concentrations are presented as supplementary data (Supplementary Table 2). Proteins were detected using 3, 3′-Diaminobenzidine and H_2O_2 as the substrate solution. Band intensity was measured using ImageJ software after subtraction of background and band density normalization.

Measurement of Catalase (CAT) Activity

CC homogenates were centrifuged at 8000 (4 °C for 10 min), and supernatants were mixed with reaction medium including H_2O_2 (10 mM), and sodium phosphate buffer (50 mM, pH 7.0). Finally, CAT activity was measured by absorbance decrease at 240 nm in a microplate reader. H_2O_2 (1 M) consuming rate per min defined one unit of the enzyme [22].

Measurement of Superoxide Dismutase (SOD) Activity

SOD activity was measured based on the ability to generate superoxide radicals by xanthine and xanthine oxidase which produces a red formazon dye following reaction with 2-(4-iodophenyl)-3-(4-nitrophenol)-5-phenyltetrazolium chloride (INT). The inhibition degree of this reaction was considered as SOD activity in the CC homogenates. One unit of SOD activity was defined as the amount of enzyme that inhibits the rate of INT reduction by 50% [23].

Measurement of Glutathione Peroxidase (GPx) Activity

Following centrifugation, 10µL of CC supernatant was mixed with 100 µL Tris-HCl (1 M, pH 8.0) as the reaction solution containing EDTA (5 mM), 20 µL of GSH (0.1 M), 100 µL of GSH reductase solution (10 units mL^{-1}), 100 µL of NADPH (2 mM), 650 µL of distilled water, 10 µL of tert-butyl hydroperoxide (7 mM). NADPH oxidation at 37 °C was assessed using a spectrophotometer at 340 nm. One unit of activity was defined as the amount of GPx required to oxidize 1 µM of NADPH per min [24].

Measurement of Lipid Peroxidation (LPO)

The Malondialdehyde (MDA) level was estimated using thiobarbituric acid reactive substances (TBARS) assay. To detect the extent of lipid peroxidation (LPO) following tissue centrifugation, CC supernatants were mixed with

thiobarbituric acid (TBA, 0.67% w/v) heated for one hour in a boiling water bath of 95–98 °C. After adding n-butanol, TBA reactive substances (TBARS) adducts were isolated by vigorous shaking. Finally, the absorbance was read at 532 nm after centrifugation of the mixture. Tetraethoxypropane standard solutions were used for calibration [25].

Measurement of Total Thiol (SH) Molecules

After centrifugation of CC homogenates, the supernatants were mixed with 200 µL of Tris-EDTA buffer containing of (0.25 M) Tris base, and (20 mM) EDTA (pH 8.2) and then were added to 4 µL of DTNB (5, 5-dithiobis-2-nitrobenzoic acid) (10 mM) in methanol. The color was appeared after 30 min incubation at 37 °C. A microplate reader was used to read the optical density of the supernatant at 412 nm against the blank [26].

Measurement of Ferric-Reducing Antioxidant Power (FRAP)

For antioxidant power estimation, following tissue centrifugation, 30 µL of CC homogenates were added to a working solution consisted of 25 mL of 0.3 M sodium acetate buffer (pH 3.6), 2.5 mL of 10 mM tripyridyl triazine (TPTZ), 2.5 mL of 20 mM $FeCl_3.H_2O$ and 42 µL of DI water. Samples were homogenized and kept in the dark for half an hour at 37 °C, followed by10 min cooling. Finally, the absorbance of the samples was measured in duplicate at 593 nm in a microplate reader (SpectranMax 190, Molecular Devices, USA). Antioxidant capacity was presented as mM of FeII equivalents calculated from a $FeSO_4$ (0.0156 to 0.375 mM) standard curve of known concentration and normalized by the amount of protein (FeII equivalent mM μg^{-1}protein) in the sample [23].

Determination of Total Glutathione (tGST) Activity

To determine total glutathione 20 µL of CC supernatants (after centrifuge at 8000×*g* at 4 °C for 10 min) were transferred to a 96-well microplate followed by addition of 120 µL of 1.68 mM 2-nitrobenzoic acid and 3.3 units/mL glutathione reductase (GR) prepared in 0.1 M potassium phosphate buffer with 8.8 mM EDTA disodium salt (pH 7.5). A β-NADPH buffer (60 µL, 0.8 mM) was prepared in potassium phosphate buffer with EDTA disodium salt (8.8 mM, pH 7.5) and subsequently was added to each well before measuring the absorbance (at 405 nm) every 30 s (for 5 min). Changes in absorbance/min were measured as 2-nitro-5-thiobenzoic acid formation rate. tGSH concentration was calculated using linear regression to determinate values from the standard curve [27].

In-Silico Analysis

Molecular docking was performed using AutoDoc4 (https://autodock.scripps.edu). The 3-D structure of each promoter was obtained using the make_na server (https://structure.usc.edu/make-na/server.html) based on their sequences. To obtain natural DNA molecule structures, a 20 ns molecular dynamics simulation was conducted in aqueous medium and standard condition using Gromacs 5.1.1 software (https://www.gromacs.org). The drug structure was mapped using ACD/LAB software (https://www.acdlabs.com), and then its 3D coordinates were obtained in Avogadro software. Energy minimization and final optimization of the structure were also performed using the steep algorithm in Avogadro (https://avogadro.cc). Atomic charges and typing, in addition to torsion settings, were conducted in the MGL tools package (https://mgltools.scripps.edu). The energetic maps for all involved atom types were calculated in AutoGrid4. Final docking was done using Autodack4 software, in 200 runs under the Lamarckian genetic algorithm. List of IAPs and their specific domains besides the structure of YM155 docked in DNA is shown in Fig. 2.

Statistical Analysis

All analyses were done using the GraphPad Prism 6 software (GraphPad Instat Software Inc., USA). Two-way analysis of variance (ANOVA) with Bonferroni post hoc test was carried out for quantitative measurement. The results were presented as mean ± SEM and value of $P < 0.05$ was considered as statistically significant.

Results

The cupYM Model Deteriorates Motor Function and Coordination

General locomotor activity (TD and velocity) and anxiety behavior (TD) were evaluated in an open-field experiment (Fig. 3a–d). As predicted, the three-week cup challenge did not significantly decrease TD, velocity, DC and DC/TD ratio, as compared to the control group (Fig. 3a–d). Co-administration of cup and YM155 (cuYM model) notably decreased mice TD ($P < 0.05$), velocity ($P < 0.01$), DC ($P < 0.05$) and DC/TD ratio ($P < 0.01$) compared to the cup group (Fig. 3a–d). On the other hand, treatment of healthy mice with YM155 alone did not significantly affect open-field parameters compared to the control group (Fig. 3a–d). Three-week cup administration did not cause any change in the number of falls compared to the control group (Fig. 3e–g). Instead, the cuYM group fell more frequently and had notably weaker motor coordination compared to

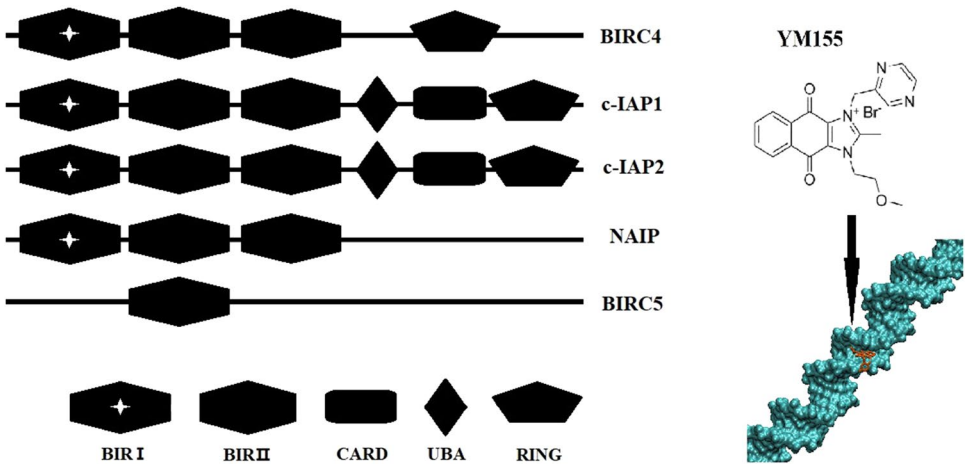

Fig. 2 List of IAPs and their specific domains besides structure of YM155 docked in DNA

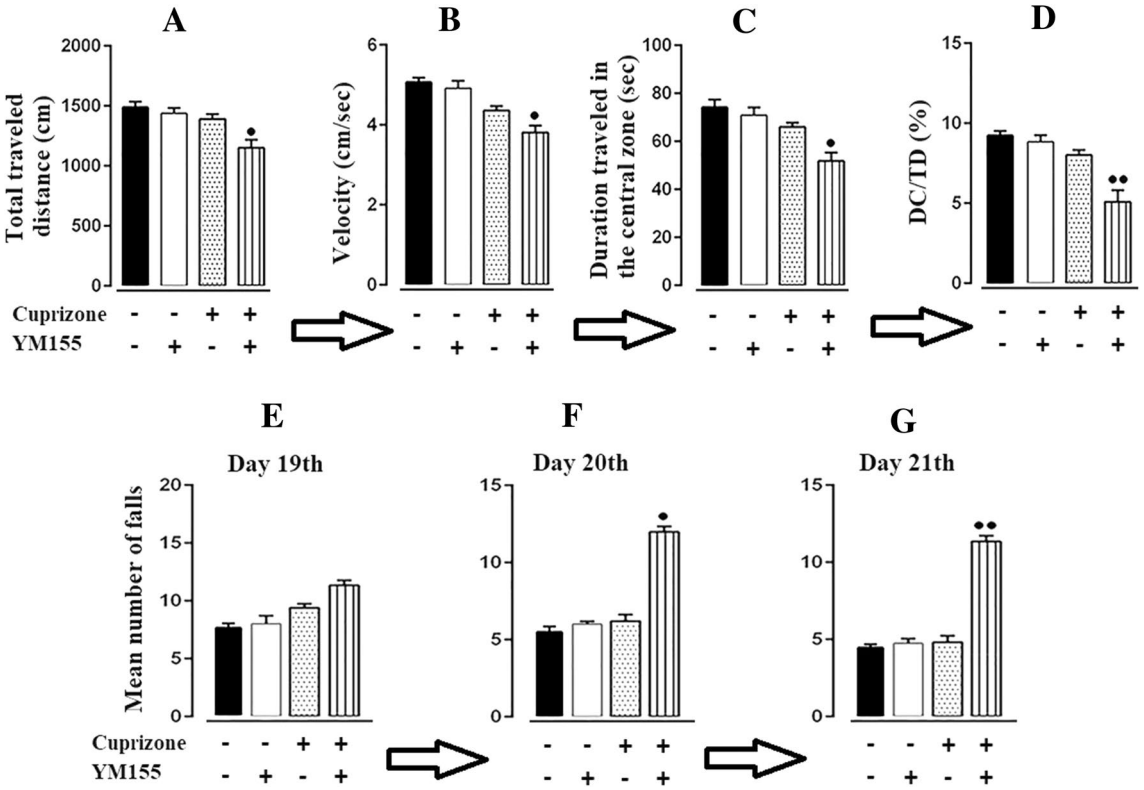

Fig. 3 The effects of cuYM on the mice behavior parameters in the Open-field test (**a**–**d**) and on the number of mice falls in the Rota-rod test (**e**–**g**). The behavioral measurements (N = 10 in each group) were made at time points 21th (Open-field) or 19th, 20th and 21th (Rota-rod) after start point. Mice in cuYM group (cuprizone + YM155) traveled shorter distances with lower velocities, spent fewer times in the central zone and had lover DC/DT ratio compared to the other groups (**a**–**d**). The graph shows the number of falls in three different consecutive trials on the experiment days (**e**–**g**). Only mice in cuYM group had significantly weaker motor coordination than cup group at both 20 and 21th day (**e**–**g**). Data represent the mean ± S.E.M analyzed by two-way ANOVA. $^{\bullet}P < 0.05$ and $^{\bullet\bullet}P < 0.01$ compared to cup mice with Bonferroni's correction for multiple comparisons

the cup group on their second (day 20th) and third (day 21st) trials ($P < 0.05$, and $P < 0.01$ respectively, Fig. 3e–g). Treatment of healthy mice with YM155 alone did not significantly affect the number of falls compared to the control group (Fig. 3e–g).

The cupYM Model Significantly Increased Intrinsic Apoptosis and Decreased Some AIPs

The results showed that three-week cup treatment increases mRNA and protein expression of caspase-3 ($P < 0.001$)

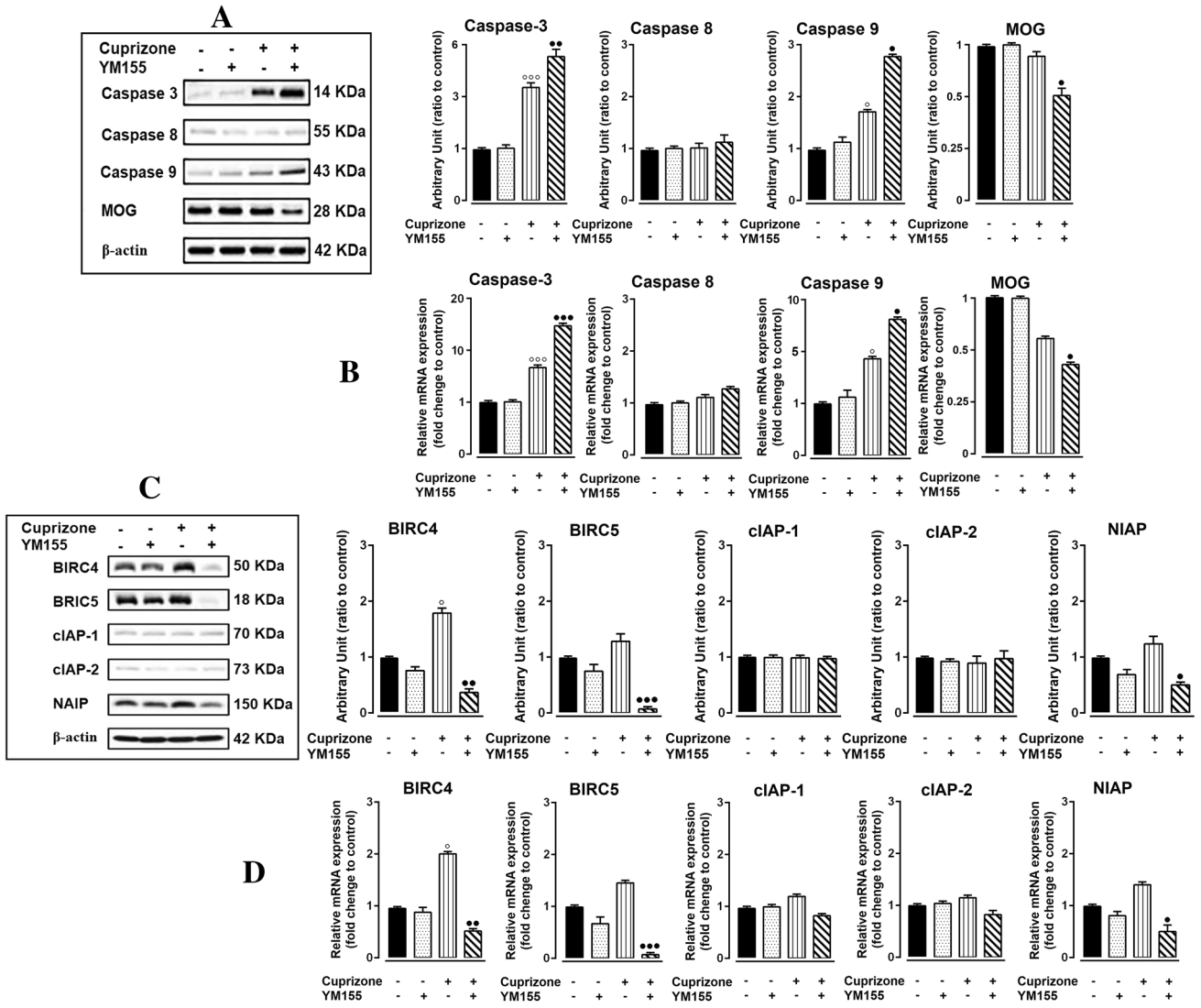

Fig. 4 The effects of cupYM on the protein and mRNA expression of caspases (3, 8 and 9), MOG and apoptosis-inhibiting proteins (BIRC4, BIRC5, cIAP-1, cIAP-2 and NIAP). First, the data normalized with the internal control (β-actin) and then indicated as fold change to the control group (N = 4 in each group). Data represent the mean ± S.E.M analyzed by two-way ANOVA. $^{\circ}P<0.05$ and $^{\circ\circ\circ}P<0.001$ compared to control mic $^{\bullet}P<0.05$, $^{\bullet\bullet}P<0.01$ and $^{\bullet\bullet\bullet}P<0.001$ compared to cup mice with Bonferroni's correction for multiple comparisons

and caspase-9 ($P<0.01$) compared to the control group, stimulating the mitochondrial pathway induction of apoptosis (Fig. 4a, b). Cuprizone treatment had no significant effect on mRNA and protein expression of caspase-8, showing no apoptosis induction from the extrinsic pathway (Fig. 4a, b). Although mRNA and protein expression of caspase-3 ($P<0.001$ and $P<0.01$ respectively) and caspase-9 ($P<0.01$) in the cuYM group were increased compared to the cup group, YM155 alone did not significantly influence mRNA and protein expression of caspases in the control group (Fig. 4a, b). The cupYM model exhibited the most inductive effect on the expression of caspase-3 and caspase-9 mRNA and protein (Fig. 4a, b). According to the above-mentioned results, YM155 can directly exacerbate the effect of cup via the induction of the mitochondrial pathway of apoptosis. For a better understanding of apoptosis effectors, the effect of cuYM was investigated on mRNA and protein expression of apoptosis-inhibiting proteins (AIPs). In the cup group, mRNA and protein expression of BIRC4 were significantly increased, while BIR5 and NIAP were not significantly augmented compared to the control group, indicating activation of endogenous anti-apoptotic pathways (Fig. 4c, d). Remarkably, in addition to the down-regulation of BIRC5, the expressions of BIRC4 and NIAP were also reduced at both mRNA and protein levels in the cupYM group (Fig. 4c, d). Noteworthy, the results showed

that three weeks of cupYM treatment significantly reduces mRNA and protein expression of BIRC5 ($P < 0.001$), BIRC4 ($P < 0.01$) and NIAP ($P < 0.05$) compared to the cup group (Fig. 4c, d). YM155 had a great inhibitory effect on mRNA and protein expression of BIRC5, followed by BIRC4 and NIAP, respectively (Fig. 4c, d). Changes in the protein and mRNA expression of cIAP-1 and cIAP-2 were not significant either under the influence of cup or under the influence of YM155 (Fig. 4c, d). According to the above-mentioned results, YM155 as a specific blocker of BIRC5 can also affect mRNA and protein expression of other IAPs such as BIRC4 and NIAP.

The cupYM Model Significantly Boosted Cup-Induced Elimination of Mature OLGs and Myelin Loss

The effect of cupYM treatment was investigated on the expression of MOG mRNA and protein by RT-PCR method (Fig. 4a, b). The results showed that three-week cup treatment inadequately reduces mRNA and protein expression of MOG compared to the control group, which indicates the limited elimination of mature OLGs (Fig. 4a, b). YM155 had no significant effects on mRNA and protein expression of MOG in control groups (Fig. 4a, b). As expected, cupYM significantly reduced mRNA ($P < 0.05$) and protein ($P < 0.05$) expression of MOG, showing the widespread removal of mature OLGs (Fig. 4a, b). According to the above-mentioned results, YM155 can directly worsen the cup effects and induce mature OLGs damage. In order to confirm the acceleration of mature OLGs destruction by cupYM, immunohistochemistry assay was used to simultaneously examine the expression of MOG, as a particular marker of adult OLGs, and cleaved-caspase-3, as an endpoint marker of the apoptosis (Fig. 5a). The results showed that three-week cup consumption significantly increases the number of cleaved-caspase-3^+ cells ($P < 0.01$) and cleaved-caspase-3^+/MOG^+ ($P < 0.01$) double positive cells, but had no recognizable effects on the number of MOG^+ cells, indicating the occurrence of insufficient death signaling in the mature OLGs (Fig. 5a). The YM155 compound had no hazardous effects on either MOG^+ or cleaved-caspase-3^+ cells in control groups (Fig. 5). As expected, cupYM significantly increased the number of MOG^+ cells ($P < 0.05$) and a number of cleaved-caspase-3^+/MOG^+ double positive cells ($P < 0.05$), pointing to the presence of extensive apoptosis in mature OLGs in comparison with the cup group (Fig. 5a). Moreover, sections from CC region of each group were stained with LFB in order to stain the lipid-rich myelin as blue (Fig. 5b). As predicted, even after three weeks cup treatment alone, myelin level did not significantly change compared to the control group (Fig. 5b). Administration of cup in conjunction with YM155 (cupYM group/model) for three weeks had a statistically significant ($P < 0.05$) negative effect on LFB density compared to the cup alone group (Fig. 5b). According to the above results, YM155 potentially can exacerbate the effect of the cup and induce the specific apoptosis of mature OLGs and demyelination.

The cupYM Model Considerably Increased Brain Oxidative Stress

In order to examine the effects of cupYM on typical oxidative stress parameters, we determined CAT, SOD, GPx, MDA, SH, FRAP and tGSH levels in brain homogenates from the corpus callosum region. As shown in Table 1, CAT and SOD levels were significantly reduced after cup feeding ($P < 0.05$) compared to the control group. These effects were also significantly enhanced in the cupYM group ($P < 0.05$, Table 1). On the other hand, GPx, MDA, SH, FRAP and tGSH levels were not significantly changed in cup group compared to the control group. Interestingly, cupYM administration significantly increased MDA ($P < 0.05$) and decreased GPx ($P < 0.05$) compared to the cup group (Table 1). Administration of cupYM did not affect SH, FRAP and tGSH levels in comparison with the cup group (Table 1).

The cupYM Model Interrupted BIRC4, BIRC5 and NIAP Promoters in Certain TF Binding Motifs

To exactly describe direct or indirect effects of cupYM on mRNA and protein expression of altered genes (BIRC4, BIRC5, and NAIP), the interaction of this small molecule (YM155) with each certain mouse promoter sequence (duplex, helix type B) was evaluated via molecular modeling and docking analysis. The promoter sequence data used in this article could be found in the eukaryotic promoter database (EPD) libraries under the following promoter IDs: Xiap_1, Xiap_2, Xiap_3 and Xaf1_1 for BIRC4; Birc5_1 for BIRC5; Naip1_1, Naip2_1, Naip5_1, and Naip6_1 for NAIP from sequence -50 to + 10. EPD is an annotated collection of eukaryotic promoters for which the transcription starts site (TSS) has been experimentally determined. Therefore, to analyze the interaction between YM155 and the promoter of the selected genes, EPD was employed in order to access to updated promoter sequences. Binding energy of YM155 attachment to specific DNA sequences (clusters) in each promoter was calculated and the position of transcription factor (TF) binding motifs in the interrupted clusters were further reported (Figs. 6, 7, 8 and Tables 2, 3, 4). Two-dimensional docking pose of the complex of BIRC4 promoter sequences and YM155 is shown in Fig. 6. Analysis of molecular interactions showed that YM155 has a relatively high affinity

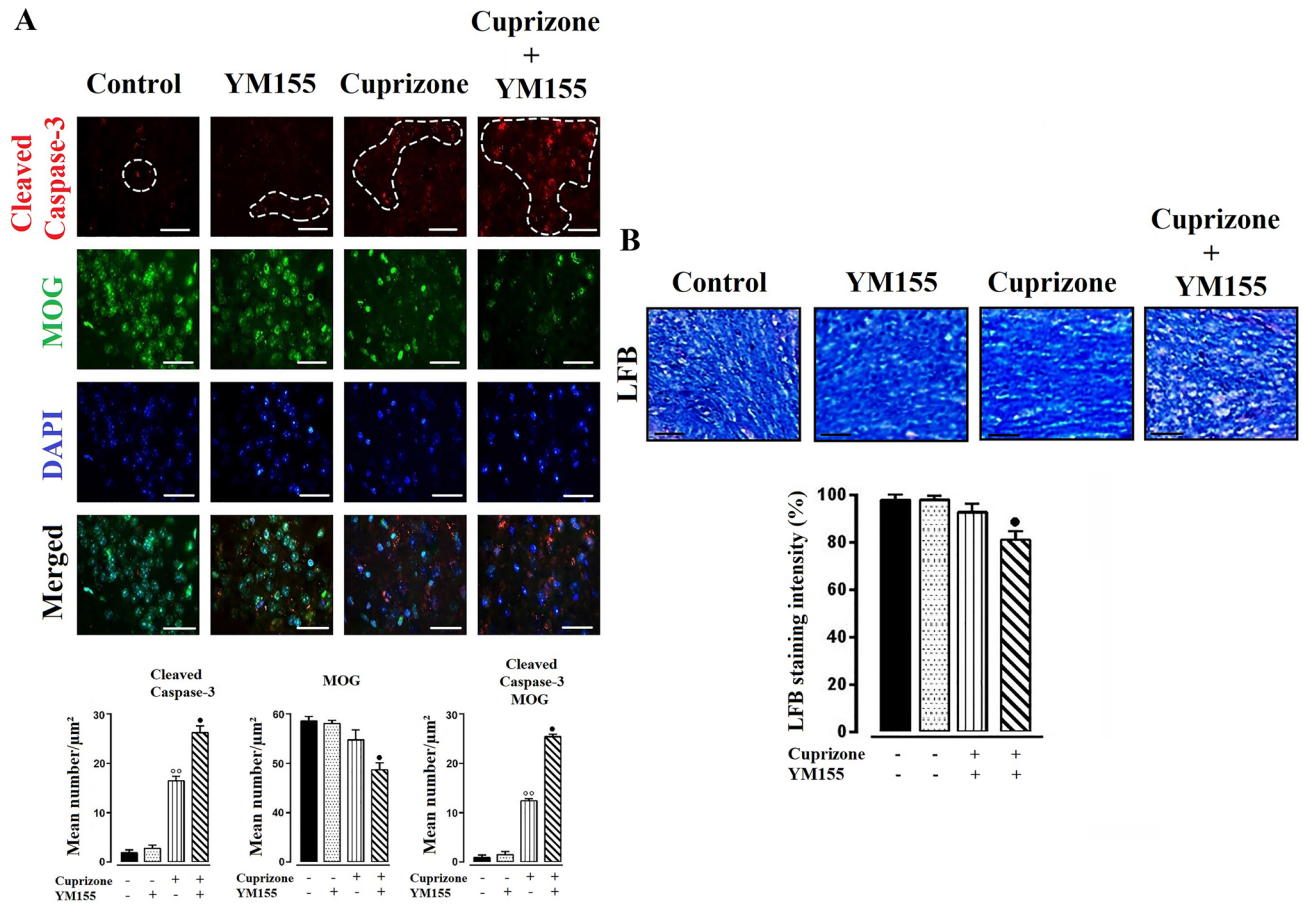

Fig. 5 Effects of cupYM on the population of the cleaved-caspase-3$^+$/MOG$^+$ positive cells (**a**) and myelin quantity (**b**). Double staining for cleaved-caspase-3 and MOG were performed in the midline corpus callosum and immunofluorescence signals (red for cleaved-caspase-3$^+$ and green for MOG$^+$) from each independent group were counted, their mean was calculated and data reported as a mean number per µm^2 (N = 4 in each group). LFB staining were performed in the midline corpus callosum and myelin amount from each independent group was counted, their mean was calculated and data reported as an intensity (N = 4 in each group). Scale bar = 50 µm. Data represent the mean ± S.E.M analyzed by two-way ANOVA. °°$P < 0.01$ compared to control mic •$P < 0.05$, compared to cup mice with Bonferroni's correction for multiple comparisons

Table 1 Effects of YM155 administration in biochemical parameters of mice brain antioxidant status

Parameters	Experimental groups			
	Control + Vehicle	Control + YM155	Cuprizone + Vehicle	Cuprizone + YM155
CAT (Unit/mg)	49.21 ± 2.51	47.25 ± 2.66	42.34 ± 1.26*	35.34 ± 3.46**
SOD (Unit/mg)	50.50 ± 4.61	48.43 ± 3.73	39.72 ± 2.31*	28.41 ± 2.21**
GPx (Unit/mg)	250.16 ± 9.22	245.79 ± 6.52	239.32 ± 4.61	214.11 ± 5.34**
MDA (nmol/g)	1.29 ± 0.13	1.56 ± 0.17	1.98 ± 0.46	2.55 ± 0.38**
SH (mmol/g)	55.12 ± 4.18	54.24 ± 4.49	49.52 ± 3.44	45.12 ± 2.03
FRAP (µmol/g)	7.3 ± 0.98	7.5 ± 1.24	8.2 ± 1.54	10.1 ± 1.73
tGSH (µmol/g)	25.34 ± 0.42	24 ± 2.81	21 ± 3.53	20 ± 1.26

Parameters are expressed as mean ± S.E. values

SOD superoxide dismutase, *GPx* glutathione peroxidase, *CAT* catalase, *tGSH* total glutathione, *FRAP* ferric reducing antioxidant power, *MDA* malondialdehyde, *SH* thiol groups

*P < 0.05, compared to the control group

**P < 0.05, compared to the cuprizone group

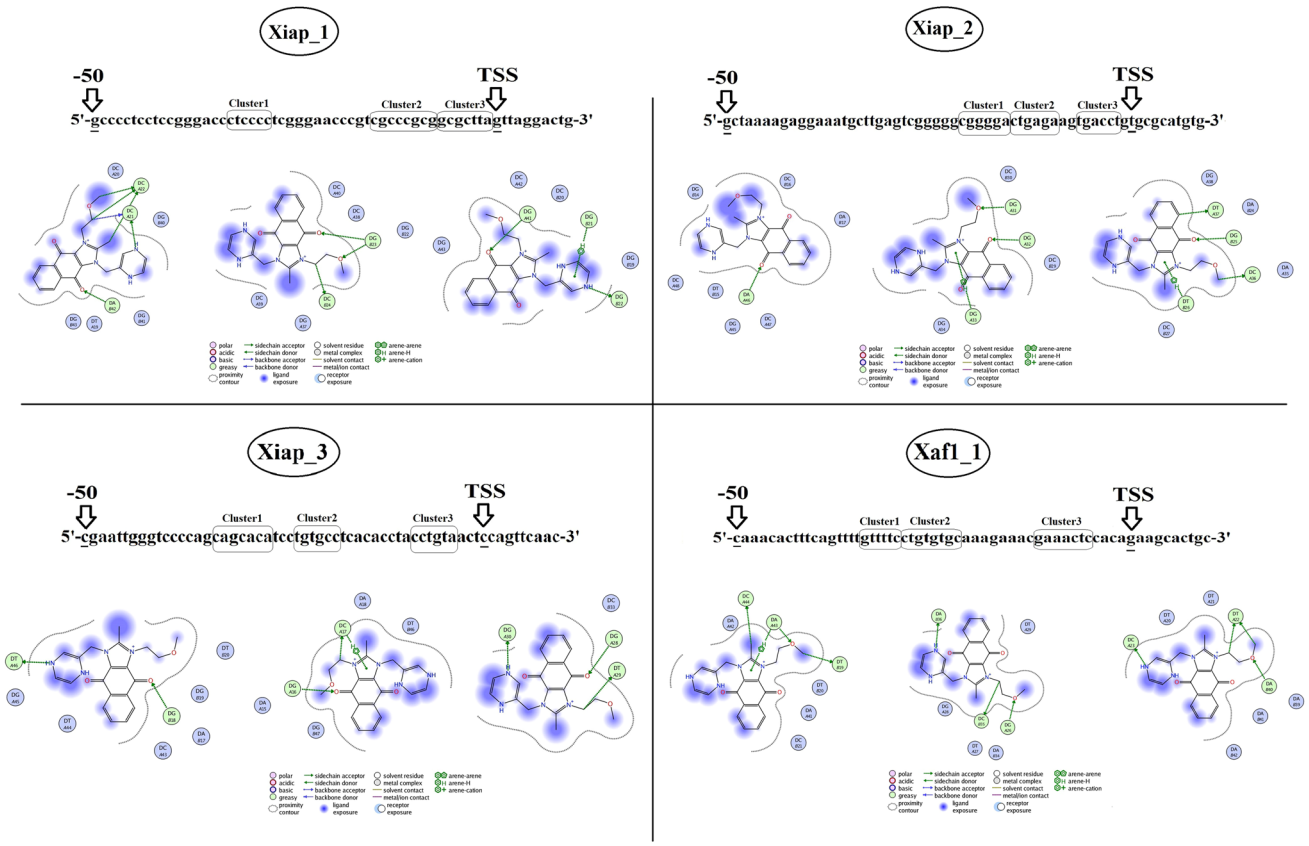

Fig. 6 YM155 docked in the four promoter sequences of BIRC4 (Xiap_1, Xiap_2, Xiap_3, and Xaf1_1). The two-dimensional docking pose of the DNA (promoter sequence) and YM155 complex showed in the below of sequences. YM155 different binding pockets on each promoter indicated as cluster 1 to 3 with detail information

with all BIRC4 promoter sequences. The highest bonding energy belonged to YM155 and cluster 1 of Xiap_1, and the lowest binding energy belonged to YM155 and cluster 3 of Xiap_1 (Table 2). Data obtained from the EPD database showed that several TFs binding motifs are interrupted with YM155 in BIRC4 promoter clusters. Among these motifs, the binding motifs of certain TFs belonged to important families such as krüppel-like family (Klf1/5/9), specificity proteins (SP1/3/4), myeloid zinc fingers (MZF1), zinc finger proteins (ZNF740) and transcription factor activating enhancer binding protein 2 alpha (TFAP2A) which have been interrupted at least on two clusters (Table 2). Two-dimensional docking pose of the complex of BIRC5 promoter sequences and YM155 are shown in Fig. 7. Molecular interaction analysis demonstrated that YM155 has a relatively high affinity with all BIRC5 promoter sequences. The highest binding energy belonged to YM155 and cluster 2, while the lowest was related to YM155 and cluster 3 of Birc5_1 (Table 3). Data obtained from the EPD database showed that lover TFs binding motifs are interrupted with YM155 in BIRC5 compared to BIRC4 promoter clusters. Among these motifs, binding motifs of broad-complex, tram-track and bric à bracs (ZBTB33) TF were also interrupted on Xiap_1 cluster 3 (Table 2). Two-dimensional docking pose of the complex of NAIP promoter sequences and YM155 is illustrated in Fig. 8. Analysis of molecular interactions showed that YM155 has a relatively high affinity with all NAIP promoter sequences. The highest bonding energy belonged to YM155 and cluster 1 and 2 of Naip1_1, and cluster 1 of Naip6_1, and the lowest bonding energy belonged to YM155 and cluster 4 of Naip2_1 (Table 4). Data obtained from the EPD database showed that several TFs binding motifs are also interrupted with YM155 in NAIP promoter clusters, among which binding motifs of TFs such as Sry-related HMG boxes (Sox3), Paired box (Pax2), and Gata4 were interrupted on at least two clusters (Table 4). Immune-system related transcription factors such as interferon regulatory factors (IRFs), signal transducer and activator of transcription (STATs), and nuclear

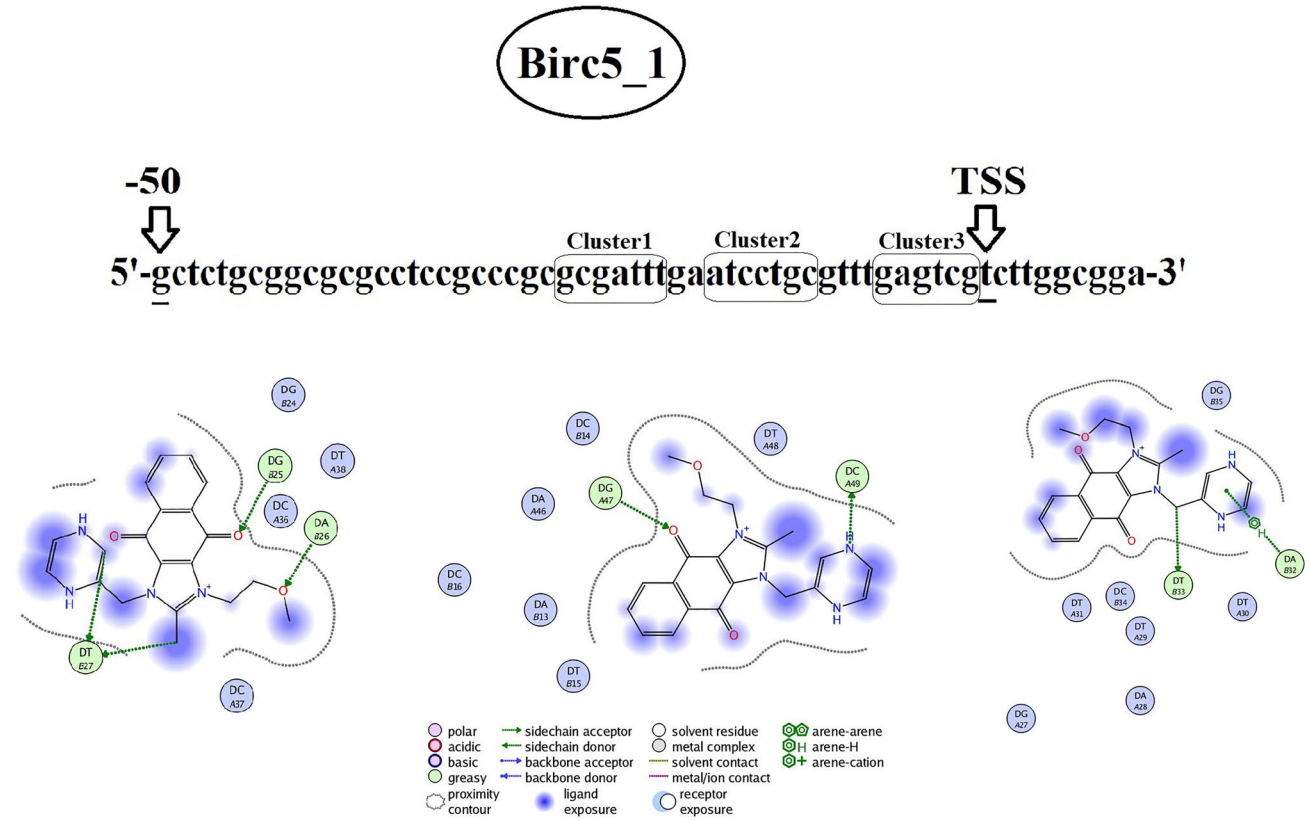

Fig. 7 YM155 docked in the one promoter sequence of BIRC5 (Birc5_1). The two-dimensional docking pose of the DNA (promoter sequence) and YM155 complex showed in the below of sequence. YM155 has three different binding pockets on the promoter that indicated as cluster 1 to 3 with detail information

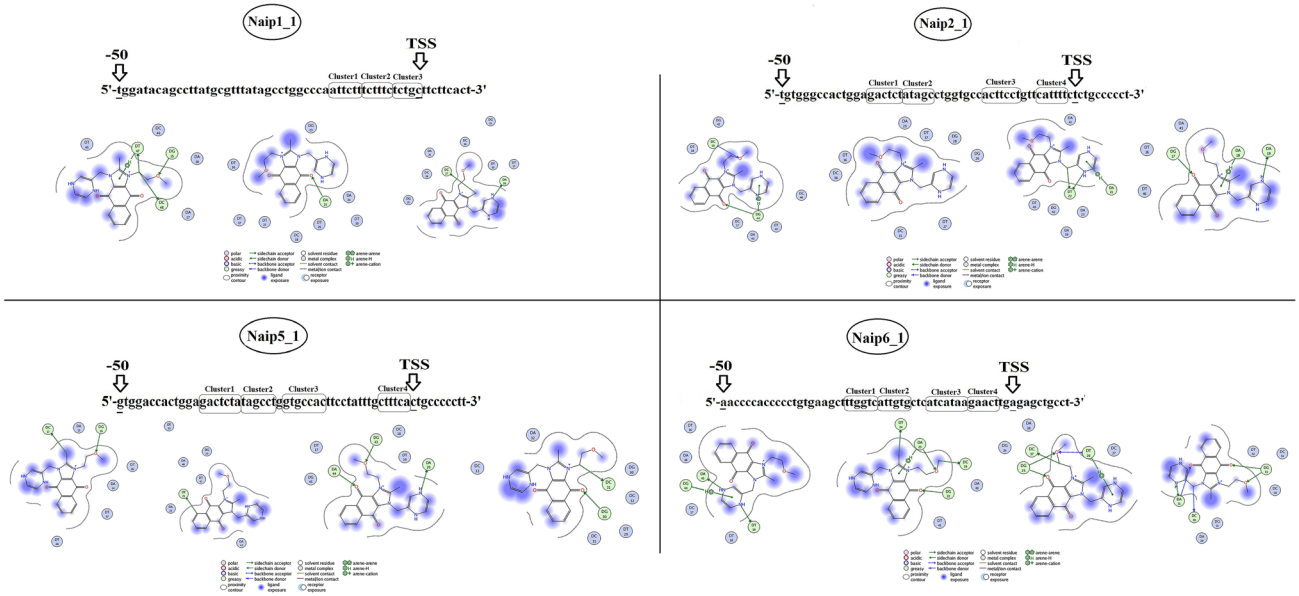

Fig. 8 YM155 docked in the four promoter sequences of NAIP (Naip1_1, Naip2_1, Naip5_1, and Naip6_1). The two-dimensional docking pose of the DNA (promoter sequence) and YM155 complex showed in the below of sequences. YM155 different binding pockets on each promoter indicated as cluster 1 to 4 with detail information

Table 2 Molecular interactions of YM155 with BIRC4 promoters and possible interrupted transcription factors

BIRC4 promoters (PID)	Binding energy of attachment of YM155 to specific DNA sequences (clusters)						Position of transcription factor (TF) motifs in interrupted clusters		
	Cluster1		Cluster2		Cluster3				
	VDW	EE	VDW	EE	VDW	EE			
	kcal/mol						Cluster1	Cluster2	Cluster3
Xiap_1 (NM_009688)	− 6.53	− 0.18	− 6.42	− 0.21	− 5.82	− 0.12	**(− 33 to − 28)**	**(− 15 to − 8)**	**(− 7 to − 1)**
	Total = − 6.71		Total = − 6.63		Total = − 5.94		Nfkb2(− 33), **Klf1**(− 32)/2(− 30)/4(− 30)/**5**(− 31)/6(− 31)/8(− 30)/**9**(− 31), **SP1**(− 31)/**3**(− 31)/**4**(− 31), **MZF1**(− 29), **ZNF740**(− 29), ZIC3(− 28)	E2F4(− 15), NRF1(− 11), **TFAP2A**(− 8,− 9,− 10)/2B(− 8,− 9,− 10)/2C(− 8,− 9,− 10), ZIC1(− 10)/4(− 10)	**ZBTB33**(− 7)
Xiap_2 (NM_009688)	− 6.36	− 0.05	− .6.11	− 0.14	− 5.92	− 0.21	**(− 21 to − 16)**	**(− 15 to − 10)**	**(− 7 to − 2)**
	Total = − 6.41		Total = − 6.25		Total = − 6.13		**Klf1**(− 19)/**5**(− 20)/**9**(− 20)/14(− 21)/16(− 20), **ZNF740**(− 21), **SP1**(− 20)/**3**(− 20)/**4**(− 20)/8(− 21), **HIC2**(− 18), TFDP1(− 18) **MZF1**(− 17)	**ZNF263**(− 15), **Gata4**(− 11)	**NR1H4**(− 5), **NR2F1**(− 4)/**F2**(− 3), **NR4A1**(− 3)/**A2**(− 4), **Pax2**(− 6), **RORA**(− 2)
Xiap_3 (NM_009688)	− 6.27	− 0.25	− 6.19	− 0.11	− 6.14	− 0.18	**(− 34 to − 28)**	**(− 24 to − 19)**	**(− 9 to − 4)**
	Total = − 6.52		Total = − 6.3		Total = − 6.32		**TFAP2A** (− 34), ASCL1(− 33)	TFE B(− 22)/C(− 23), Zfx(− 22), FOSL2(− 19), PBX3(− 20)	SNAI2(− 7), SCRT1(− 6) RXRB(− 5), T(− 9), TBX19(− 9)
Xiaf1_1 (NM_001291153)	− 6.56	− 0.11	− 6.18	− 0.32	− 6.1	− 0.16	**(− 33 to − 28)**	**(− 27 to − 20)**	**(− 11 to − 5)**
	Total = − 6.67		Total = − 6.5		Total = − 6.26		**STAT2**(− 33), **Sox3**(− 32)/**6**(− 32)/**15**(− 32), Foxj2(− 31)/3(− 30), Foxg1(− 31), Foxk1(− 31)/2(− 30), Foxp1(− 31)/2(− 30), Foxo1(− 31)/4(− 30)/6(− 30), Foxd3(− 30), Foxc2(− 30), Foxf2(− 29), **FLI1**(− 28)	SPIB(− 26), ELF1(− 27), ETV2(− 27), Foxa1(− 22)	RELA(− 7), Stat5b(− 2), ZNF354C(− 3), **IRF1**(− 11)/4(− 11)/7(− 11)

Bolded TFs indicate interrupted in other promoters

Bold numbers indicate position of cluster in DNA

PID Promoter ID, *VDW* van der Waals interactions, *EE* electrostatic interactions, *kcal/mol* kilocalorie *per* mole, *Bolded TFs* interrupted in other promoters

Table 3 Molecular interactions of YM155 with BIRC5 promoter and possible interrupted transcription factors

BIRC5 Promoters (PID)	Binding energy of attachment of YM155 to specific DNA sequences (clusters)						Position of transcription factor motifs in interrupted clusters		
	Cluster1		Cluster2		Cluster3		Cluster1	Cluster2	Cluster3
	VDW (kcal/mol)	EE (kcal/mol)	VDW (kcal/mol)	EE (kcal/mol)	VDW (kcal/mol)	EE (kcal/mol)			
Bric5_1 (NM_009689)	− 6.38	− 0.17	− 6.22	− 0.12	− 5.48	− 0.21	(**− 26 to − 20**)	(**− 17 to − 11**)	(**− 6 to − 1**)
	Total = − 6.21		Total = − 6.34		Total = − 5.69		CENPB(− 23), E2F7(− 25), Hes1(− 25), **ZBTB33**(− 25), Tcfl5(− 25, − 26)	–	PROX1(− 1), JDP2(− 3)

Bolded TFs indicate interrupted in other promoters

Bold numbers indicate position of cluster in DNA

PID Promoter ID, *VDW* van der Waals interactions, *EE* electrostatic interactions, *kcal/mol* kilocalorie *per* mole, *Bolded TFs* interrupted in other promoters

receptors (NRs) were interrupted on a wide range in several clusters of the target genes (Tables 2, 3, 4).

Discussion

CNS contains millions of neurons connected by nerve fibers and axons, transmitting nerve impulses through the body. Originating from the oligodendroglia cells in the CNS, the myelin sheath is an extended and reformed membrane wrapped around the nerve axon. Cup is frequently employed in the toxic-induction of de- and remyelination, and molecular modeling of MS lesions [4]. The degree of demyelination in the cup model may be variable, hence the difficulty associated with determining the time of de- and remyelination. Our previous work demonstrated that the best time for cellular and molecular monitoring of active demyelination and activation of autonomous repair is between weeks 5 to 6 of cup administration [28]. Accordingly, the optimal time to conduct therapeutic interventions is during the last week of model induction (week 6), when the maximum damage is induced and minimum variations in the lesion are measurable. It has been confirmed that OLGs loss during feeding with the cup is mediated by the induction of redox imbalance and activation of endogenous apoptosis signals [29]. Oxidative stress and ROS production entail lipid peroxidation, and the end product of lipid peroxidation (MDA) reduces the respiratory activity of mitochondria, and reacts with cysteine, histidine, and lysine, resulting in protein degradation and loss of enzymatic function [24]. OLGs remarkably influence processes which are dysregulated in different psychiatric (schizophrenia and bipolar disorders) and neurodegenerative diseases, including nerve impulse conduction and ionic homeostasis. Furthermore, OLGs, like other cell types, have their particular endogenous molecular protective systems to either prevent or delay programmed cell death. Moreover, signaling pathways such as AIPs could delay cell death and allow for functional recovery following injuring [30].

Sepantronium bromide (YM155) is one of the favorable inhibitors of BIRC5/survivin (with an IC50 of 0.54 nM) showing suitable toxicity in patients with advanced solid malignancies [20, 31]. However, Glaros et al. observed that YM155 eradicates tumor cells primarily by inducing DNA damage and not by direct BIRC5 inhibition [32]. YM155 is highly hydrophilic and has a permanent cationic charge on one of its nitrogen atoms with a short plasma half-life of approximately 1–2 h, as determined in pharmacokinetic measurements in experimental animals [33]. Safety and tolerability of YM155 have been confirmed in several clinical trials and in a variety of malignancies [34–38].

In our proposed model of OLGs loss, it was observed that YM155 negatively influences the cup-induced behavioral deficits (Fig. 3), and promotes neuropathological changes (Figs. 4 and 5). As shown in Fig. 3, cupYM model deteriorated motor function and coordination, indicating that the suppression of Survivin/BIRC5 signaling has a negative effect on cup-induced behavioral deficits and motor dysfunction. These adverse effects could be due to downregulation of endogenous anti-apoptosis mediators and its signal transduction in OLGs.

Based on previous studies, in the classical model, OLGs apoptosis (caspase-3^+ OLGs) commences as early as a week following cup treatment in the most affected regions (i.e. midline corpus callosum), while demyelination (with LFB staining) is well-visualized only after 5 weeks of treatment [39]. Therefore, the time point selected in this study is

Table 4 Molecular interactions of YM155 with NAIP promoters and and possible interrupted transcription factors

NAIP Promoters (PID)	Binding energy of attachment of YM155 to specific DNA sequences (clusters)								Position of transcription factor motifs in interrupted clusters			
	Cluster1		Cluster2		Cluster3		Cluster4					
	VDW	EE	VDW	EE	VDW	EE	VDW	EE				
	kcal/mol								Cluster1	Cluster2	Cluster3	Cluster4
Naip1_1 (NM_008670)	− 6.26	− 0.23	− 6.32	− 0.17	− 5.64	− 0.16	–	–	**(− 16 to − 11)**	**(− 10 to − 5)**	**(− 4 to + 1)**	**(−)**
	Total = − 6.49		Total = − 6.49		Total = − 5.80		–		–	**IRF1**(− 7), **Sox3**(− 8)/**10**(− 9) **STAT2**(− 8), ZNF24(− 10)	E2F6(1) **Gata4**(− 3) SPIC(− 4) **ZNF263**(− 3)	–
Naip2_1 (NM_010872)	− 6.05	− 0.18	− 6.30	− 0.17	− 5.86	− 0.20	− 5.00	− 0.14	**(− 36 to − 31)**	**(− 30 to − 26)**	**(− 17 to − 11)**	**(− 7 to − 2)**
	Total = − 6.23		Total = − 6.47		Total = − 6.06		Total = − 5.14		Pax1(− 32) PBX1(− 32)	GLIS1(− 26)	**Gata4**(− 11) **MZF1**(− 17) RELB(− 16)	**NR2F1**(− 4)/**F2**(− 3) **NR4A1**(− 3)/**A2**(− 4), **Pax2**(− 6) **RORA**(− 2)
Naip5− 1 (NM_001033367)	− 6.22	− 0.11	− 6.21	− 0.10	− 5.78	− 0.90	− 5.73	− 0.03	**(− 37 to − 31)**	**(− 30 to − 25)**	**(− 23 to − 17)**	**(− 6 to − 1)**
	Total = − 6.33		Total = − 6.31		Total = − 6.68		Total = − 5.76		–	–	Mafk(− 18), HES7(− 23), **HIC2**(− 18), TLX1(− 22), PKNOX2(− 22),	**FLI1**(− 1), Foxa2(− 5), IRF2(− 3), PRDM1(− 3), RXRA(− 1),
Naip6_1 (ENS-MUSG00000078942)	− 6.29	− 0.20	− 6.31	− 0.15	− 5.88	− 0.19	− 5.46	− 0.18	**(− 29 to − 24)**	**(− 23 to − 18)**	**(− 14 to − 8)**	**(− 7 to − 3)**
	Total = − 6.49		Total = − 6.46		Total = − 6.07		Total = − 5.64		LEF1(− 27) **NFE2L1**(− 23) **NR1H4**(− 23) **Pax2**(− 22) Tcf7(− 26)/ l1(− 26)	**Sox3**(− 19)/**6**(− 1 9)/9(− 20)/**10**(− 20)/13(− 21)/**15** (− 19)/17(− 21), **NFE2L1**(− 23), **NR1H4**(− 23), **Pax2**(− 22)	HOXC10(− 8), Rfx1(− 9,10), TFE3(− 10),	ESRRB(− 4), SIX1(− 2)

Bolded TFs indicate interrupted in other promoters

Bold numbers indicate position of cluster in DNA

PID Promoter ID, *VDW* van der Waals interactions, *EE* electrostatic interactions, *kcal/mol* kilocalorie *per* mole, *Bolded TFs* interrupted in other promoters

suitable for capturing OLGs apoptosis. Our results provided evidence that down-regulation of AIPs (BIRC4, BIRC5, and NAIP) by YM155 (Fig. 4) as a programmed cell death accelerator and AIPs inhibitor, contributes to early OLGs apoptosis and demyelination (Fig. 5). Therefore, activation of AIPs signaling pathway may be a potential approach to overcome OLGs degeneration, recruiting OLGs survival vs. death mechanisms. In addition to down-regulation of BIRC5/survivin expression, cuYM declined NAIP and BIRC4, but not cIAP1 and cIAP2 proteins in comparison with the cup group. NAIP is the first discovered IAP and found to be missing in the spinal motor neurons, resulting in or contributing to spinal muscular atrophy. NAIP and BIRC4 have a caspase recruitment domain that inhibits caspases [30].

Through in-silico studies, we examined whether YM155 is able to exert its effect via interaction with BIRC4, BIRC5, and NAIP genes promoters. Although a precise mechanism of YM155 action is yet to be fully understood, it has been proposed that YM155 interacts with the translation initiation factor 3 (IF3)/transcription factor p54/Nuclear receptor factor (nrf) complex, and binds the specificity protein 1 (Sp1) transcription factor to the survivin core promoter [40]. Our results from in-silico analyses are in accordance with this mechanism of action, and we showed that YM155 potentially interrupts nuclear receptors (NRs) in a wide range in several clusters of the BIRC4, BIRC5, and NAIP genes (Tables 2, 3, 4). It was shown that YM155 also inhibits BIRC5 by perturbing transcription factor-DNA interactions of interleukin enhancer-binding factor 3 (ILF3) [41], nuclear factor-κB1 (NF-κB1 or p50) [42], and Non-POU domain-containing octamer-binding protein (NonO) [43]. Here we showed that several TFs binding motifs are interrupted by YM155 in NAIP promoter clusters, among which binding motifs of TFs such as Sox3, Pax2, and Gata4 were interrupted on at least two clusters (Table 4). Moreover, immune-system related transcription factors such as IRFs, and STATs were interrupted in several clusters of the BIRC4, BIRC5, and NAIP genes (Tables 2, 3, 4).

For the first time, our result suggests that cupYM model can interfere with other mechanisms to cause cellular changes in addition to apoptosis. YM155 treatment significantly increased redox signaling relative to the cup group, and the induction of oxidative stress potentially facilitates the apoptosis of OLGs in cupYM-induced demyelination. The superiority of this new model over other laboratory models of neurodegeneration is the immediate early OLGs loss after cupYM administration, and the lower involvement of the immune system. After 3 days of feeding with cup, the expression of myelin proteins caused by mature OLGs started to decrease, and was reduced by 90% after 5 weeks of cup diet [44]. In summary, BIRC5 activation in mature OLGs serves as a protective mechanism that defends against toxic demyelination through modulating caspases 9-related pathways where BIRC5 impeding with YM155 accelerates OLGs damage. Based on the findings, it can be concluded that selective down-regulation of BIRC5 by YM155 in mice during toxic demyelination promotes the degeneration of mature OLGs via the activation of intrinsic apoptosis pathway.

Taken together, the cupYM model entailed extensive OLGs loss and provided a suitable condition for early detection of the pathobiological determinants of demyelination in comparison with cuprizone treatment. Furthermore, YM155 is responsible for the hypersensitization of OLGs to cup and exhibits potent cytotoxicity against mature OLGs. A faster rate of demyelination provides a shorter period to investigate the prophylactic effects of compounds. These unique features of YM155 were conductive to the development of our new toxic model of demyelination. This new modified model can potentially be used for the evaluation of new therapeutic candidates that prevent demyelination or promote remyelination in the early phases of OLGs degeneration.

Acknowledgements The authors are grateful to all respected research staffs in the Pharmaceutical Science Research Center, Tehran University of Medical Sciences, Tehran, Iran, for their help with the study.

Funding This study was funded by University of Zabol (UOZ-GR-9517–13).

Compliance with Ethical Standards

Conflicts of interest The authors have no conflicts of interest to declare.

References

1. Lucchinetti C, Bruck W, Parisi J, Scheithauer B, Rodriguez M, Lassmann H (2000) Heterogeneity of multiple sclerosis lesions: implications for the pathogenesis of demyelination. Ann Neurol 47(6):707–717
2. Sanadgol N, Zahedani SS, Sharifzadeh M, Khalseh R, Barbari GR, Abdollahi M (2017) Recent updates in imperative natural compounds for healthy brain and nerve function: a systematic review of implications for multiple sclerosis. Curr Drug Targets 18(13):1499–1517. https://doi.org/10.2174/1389450118666161108124414
3. Sanadgol N, Golab F, Mostafaie A, Mehdizadeh M, Abdollahi M, Sharifzadeh M, Ravan H (2016) Ellagic acid ameliorates cuprizone-induced acute CNS inflammation via restriction of microgliosis and down-regulation of CCL2 and CCL3 pro-inflammatory chemokines. Cell Mol Biol 62(12):24–30. https://doi.org/10.14715/cmb/2016.62.12.5
4. Abakumova TO, Kuz'kina AA, Zharova ME, Pozdeeva DA, Gubskii IL, Shepeleva II, Antonova OM, Nukolova NV, Kekelidze ZI, Chekhonin VP (2015) Cuprizone model as a tool for preclinical studies of the efficacy of multiple sclerosis diagnosis and therapy.

Bull Exp Biol Med 159(1):111–115. https://doi.org/10.1007/s10517-015-2903-z
5. Heckers S, Held N, Kronenberg J, Skripuletz T, Bleich A, Gudi V, Stangel M (2017) Investigation of cuprizone inactivation by temperature. Neurotox Res 31(4):570–577. https://doi.org/10.1007/s12640-017-9704-2
6. Benardais K, Kotsiari A, Skuljec J, Koutsoudaki PN, Gudi V, Singh V, Vulinovic F, Skripuletz T, Stangel M (2013) Cuprizone [bis(cyclohexylidenehydrazide)] is selectively toxic for mature oligodendrocytes. Neurotox Res 24(2):244–250. https://doi.org/10.1007/s12640-013-9380-9
7. Oberoi-Khanuja TK, Murali A, Rajalingam K (2013) IAPs on the move: role of inhibitors of apoptosis proteins in cell migration. Cell Death Dis 4:e784. https://doi.org/10.1038/cddis.2013.311
8. Abdel-Magid AF (2017) Modulation of the inhibitors of apoptosis proteins (IAPs) activities for cancer treatment. ACS Med Chem Lett 8(5):471–473. https://doi.org/10.1021/acsmedchemlett.7b00148
9. Silke J, Meier P (2013) Inhibitor of apoptosis (IAP) proteins-modulators of cell death and inflammation. Cold Spring Harb Perspect Biol 1:1. https://doi.org/10.1101/cshperspect.a008730
10. Varughese RK, Torp SH (2016) Survivin and gliomas: a literature review. Oncol Lett 12(3):1679–1686. https://doi.org/10.3892/ol.2016.4867
11. Xia Z, Friedlander RM (2017) Minocycline in multiple sclerosis—compelling results but too early to tell. N Engl J Med 376(22):2191–2193. https://doi.org/10.1056/NEJMe1703230
12. Hebb AL, Moore CS, Bhan V, Campbell T, Fisk JD, Robertson HA, Thorne M, Lacasse E, Holcik M, Gillard J, Crocker SJ, Robertson GS (2008) Expression of the inhibitor of apoptosis protein family in multiple sclerosis reveals a potential immunomodulatory role during autoimmune mediated demyelination. Mult Scler 14(5):577–594. https://doi.org/10.1177/1352458507087468
13. Cheung CH, Cheng L, Chang KY, Chen HH, Chang JY (2011) Investigations of survivin: the past, present and future. Front Biosci (Landmark Ed) 16:952–961
14. Zhen W, Liu A, Lu J, Zhang W, Tattersall D, Wang J (2017) An alternative cuprizone-induced demyelination and remyelination mouse model. ASN Neuro 1:1. https://doi.org/10.1177/1759091417725174
15. Guo K, Huang P, Xu N, Xu P, Kaku H, Zheng S, Xu A, Matsuura E, Liu C, Kumon H (2015) A combination of YM-155, a small molecule survivin inhibitor, and IL-2 potently suppresses renal cell carcinoma in murine model. Oncotarget 6(25):21137–21147. https://doi.org/10.18632/oncotarget.4121
16. Sanadgol N, Golab F, Mostafaie A, Mehdizadeh M, Khalseh R, Mahmoudi M, Abdollahi M, Vakilzadeh G, Taghizadeh G, Sharifzadeh M (2018) Low, but not high, dose triptolide controls neuroinflammation and improves behavioral deficits in toxic model of multiple sclerosis by dampening of NF-kappaB activation and acceleration of intrinsic myelin repair. Toxicol Appl Pharmacol 342:86–98. https://doi.org/10.1016/j.taap.2018.01.023
17. Poorebrahim M, Asghari M, Abazari MF, Askari H, Sadeghi S, Taheri-Kafrani A, Nasr-Esfahani MH, Ghoraeian P, Aleagha MN, Arab SS, Kennedy D, Montaseri A, Mehranfar M, Sanadgol N (2018) Immunomodulatory effects of a rationally designed peptide mimetic of human IFNbeta in EAE model of multiple sclerosis. Prog Neuropsychopharmacol Biol Psychiatry 82:49–61. https://doi.org/10.1016/j.pnpbp.2017.11.028
18. Sanadgol N, Golab F, Askari H, Moradi F, Ajdary M, Mehdizadeh M (2018) Alpha-lipoic acid mitigates toxic-induced demyelination in the corpus callosum by lessening of oxidative stress and stimulation of polydendrocytes proliferation. Metab Brain Dis 33(1):27–37. https://doi.org/10.1007/s11011-017-0099-9
19. Keshavarz-Bahaghighat H, Sepand MR, Ghahremani MH, Aghsami M, Sanadgol N, Omidi A, Bodaghi-Namileh V, Sabzevari O (2018) Acetyl-L-Carnitine Attenuates Arsenic-Induced Oxidative Stress and Hippocampal Mitochondrial Dysfunction. Biol Trace Elem Res 184(2):422–435. https://doi.org/10.1007/s12011-017-1210-0
20. Nakahara T, Kita A, Yamanaka K, Mori M, Amino N, Takeuchi M, Tominaga F, Kinoyama I, Matsuhisa A, Kudou M, Sasamata M (2011) Broad spectrum and potent antitumor activities of YM155, a novel small-molecule survivin suppressant, in a wide variety of human cancer cell lines and xenograft models. Cancer Sci 102(3):614–621. https://doi.org/10.1111/j.1349-7006.2010.01834.x
21. Shirazi MK, Azarnezhad A, Abazari MF, Poorebrahim M, Ghoraeian P, Sanadgol N, Bokharaie H, Heydari S, Abbasi A, Kabiri S, Aleagha MN, Enderami SE, Dashtaki AS, Askari H (2019) The role of nitric oxide signaling in renoprotective effects of hydrogen sulfide against chronic kidney disease in rats: Involvement of oxidative stress, autophagy and apoptosis. J Cell Physiol 234(7):11411–11423. https://doi.org/10.1002/jcp.27797
22. Ranjbar A, Ghahremani MH, Sharifzadeh M, Golestani A, Ghazi-Khansari M, Baeeri M, Abdollahi M (2010) Protection by pentoxifylline of malathion-induced toxic stress and mitochondrial damage in rat brain. Hum Exp Toxicol 29(10):851–864. https://doi.org/10.1177/0960327110363836
23. Pourkhalili N, Hosseini A, Nili-Ahmadabadi A, Hassani S, Pakzad M, Baeeri M, Mohammadirad A, Abdollahi M (2011) Biochemical and cellular evidence of the benefit of a combination of cerium oxide nanoparticles and selenium to diabetic rats. World J Diabetes 2(11):204–210. https://doi.org/10.4239/wjd.v2.i11.204
24. von Leden RE, Yauger YJ, Khayrullina G, Byrnes KR (2017) Central nervous system injury and nicotinamide adenine dinucleotide phosphate oxidase: oxidative stress and therapeutic targets. J Neurotrauma 34(4):755–764. https://doi.org/10.1089/neu.2016.4486
25. Bodaghi-Namileh V, Sepand MR, Omidi A, Aghsami M, Seyednejad SA, Kasirzadeh S, Sabzevari O (2018) Acetyl-l-carnitine attenuates arsenic-induced liver injury by abrogation of mitochondrial dysfunction, inflammation, and apoptosis in rats. Environ Toxicol Pharmacol 58:11–20. https://doi.org/10.1016/j.etap.2017.12.005
26. Mohammadi H, Karimi G, Seyed Mahdi R, Ahmad Reza D, Shafiee H, Nikfar S, Baeeri M, Sabzevari O, Abdollahi M (2011) Benefit of nanocarrier of magnetic magnesium in rat malathion-induced toxicity and cardiac failure using non-invasive monitoring of electrocardiogram and blood pressure. Toxicol Ind Health 27(5):417–429. https://doi.org/10.1177/0748233710387634
27. Gawryluk JW, Wang JF, Andreazza AC, Shao L, Young LT (2011) Decreased levels of glutathione, the major brain antioxidant, in post-mortem prefrontal cortex from patients with psychiatric disorders. Int J Neuropsychopharmacol 14(1):123–130. https://doi.org/10.1017/S1461145710000805
28. Sanadgol N, Golab F, Tashakkor Z, Taki N, Moradi Kouchi S, Mostafaie A, Mehdizadeh M, Abdollahi M, Taghizadeh G, Sharifzadeh M (2017) Neuroprotective effects of ellagic acid on cuprizone-induced acute demyelination through limitation of microgliosis, adjustment of CXCL12/IL-17/IL-11 axis and restriction of mature oligodendrocytes apoptosis. Pharm Biol 55(1):1679–1687. https://doi.org/10.1080/13880209.2017.1319867
29. Qian ZM, Li H, Sun H, Ho K (2002) Targeted drug delivery via the transferrin receptor-mediated endocytosis pathway. Pharmacol Rev 54(4):561–587
30. Lotocki G, Keane RW (2002) Inhibitors of apoptosis proteins in injury and disease. IUBMB Life 54(5):231–240. https://doi.org/10.1080/15216540215675
31. Kita A, Mitsuoka K, Kaneko N, Nakata M, Yamanaka K, Jitsuoka M, Miyoshi S, Noda A, Mori M, Nakahara T, Sasamata M (2012)

Sepantronium bromide (YM155) enhances response of human B-cell non-Hodgkin lymphoma to rituximab. J Pharmacol Exp Ther 343(1):178–183. https://doi.org/10.1124/jpet.112.195925
32. Glaros TG, Stockwin LH, Mullendore ME, Smith B, Morrison BL, Newton DL (2012) The "survivin suppressants" NSC 80467 and YM155 induce a DNA damage response. Cancer Chemother Pharmacol 70(1):207–212. https://doi.org/10.1007/s00280-012-1868-0
33. Kaneko N, Mitsuoka K, Amino N, Yamanaka K, Kita A, Mori M, Miyoshi S, Kuromitsu S (2014) Combination of YM155, a survivin suppressant, with bendamustine and rituximab: a new combination therapy to treat relapsed/refractory diffuse large B-cell lymphoma. Clin Cancer Res 20(7):1814–1822. https://doi.org/10.1158/1078-0432.CCR-13-2707
34. Giaccone G, Zatloukal P, Roubec J, Floor K, Musil J, Kuta M, van Klaveren RJ, Chaudhary S, Gunther A, Shamsili S (2009) Multicenter phase II trial of YM155, a small-molecule suppressor of survivin, in patients with advanced, refractory, non-small-cell lung cancer. J Clin Oncol 27(27):4481–4486. https://doi.org/10.1200/JCO.2008.21.1862
35. Lewis KD, Samlowski W, Ward J, Catlett J, Cranmer L, Kirkwood J, Lawson D, Whitman E, Gonzalez R (2011) A multi-center phase II evaluation of the small molecule survivin suppressor YM155 in patients with unresectable stage III or IV melanoma. Invest New Drugs 29(1):161–166. https://doi.org/10.1007/s10637-009-9333-6
36. Papadopoulos KP, Lopez-Jimenez J, Smith SE, Steinberg J, Keating A, Sasse C, Jie F, Thyss A (2016) A multicenter phase II study of sepantronium bromide (YM155) plus rituximab in patients with relapsed aggressive B-cell Non-Hodgkin lymphoma. Leuk Lymphoma 57(8):1848–1855. https://doi.org/10.3109/10428194.2015.1113275
37. Satoh T, Okamoto I, Miyazaki M, Morinaga R, Tsuya A, Hasegawa Y, Terashima M, Ueda S, Fukuoka M, Ariyoshi Y, Saito T, Masuda N, Watanabe H, Taguchi T, Kakihara T, Aoyama Y, Hashimoto Y, Nakagawa K (2009) Phase I study of YM155, a novel survivin suppressant, in patients with advanced solid tumors. Clin Cancer Res 15(11):3872–3880. https://doi.org/10.1158/1078-0432.CCR-08-1946
38. Tolcher AW, Mita A, Lewis LD, Garrett CR, Till E, Daud AI, Patnaik A, Papadopoulos K, Takimoto C, Bartels P, Keating A, Antonia S (2008) Phase I and pharmacokinetic study of YM155, a small-molecule inhibitor of survivin. J Clin Oncol 26(32):5198–5203. https://doi.org/10.1200/JCO.2008.17.2064
39. Steelman AJ, Zhou Y, Koito H, Kim S, Payne HR, Lu QR, Li J (2016) Activation of oligodendroglial Stat3 is required for efficient remyelination. Neurobiol Dis 91:336–346. https://doi.org/10.1016/j.nbd.2016.03.023
40. Cheng Q, Ling X, Haller A, Nakahara T, Yamanaka K, Kita A, Koutoku H, Takeuchi M, Brattain MG, Li F (2012) Suppression of survivin promoter activity by YM155 involves disruption of Sp1-DNA interaction in the survivin core promoter. Int J Biochem Mol Biol 3(2):179–197
41. Nakamura N, Yamauchi T, Hiramoto M, Yuri M, Naito M, Takeuchi M, Yamanaka K, Kita A, Nakahara T, Kinoyama I, Matsuhisa A, Kaneko N, Koutoku H, Sasamata M, Yokota H, Kawabata S (2012) Furuichi K (2012) Interleukin enhancer-binding factor 3/NF110 is a target of YM155, a suppressant of survivin. Mol Cell Proteomics 1:1. https://doi.org/10.1074/mcp.M111.013243
42. Ho SH, Ali A, Chin TM, Go ML (2016) Dioxonaphthoimidazoliums AB1 and YM155 disrupt phosphorylation of p50 in the NF-κB pathway. Oncotarget 7(10):11625–11636
43. Yamauchi T, Nakamura N, Hiramoto M, Yuri M, Yokota H, Naitou M, Takeuchi M, Yamanaka K, Kita A, Nakahara T, Kinoyama I, Matsuhisa A, Kaneko N, Koutoku H, Sasamata M, Kobori M, Katou M, Tawara S, Kawabata S, Furuichi K (2012) Sepantronium bromide (YM155) induces disruption of the ILF3/p54(nrb) complex, which is required for survivin expression. Biochem Biophys Res Commun 425(4):711–716. https://doi.org/10.1016/j.bbrc.2012.07.103
44. Goldberg J, Clarner T, Beyer C, Kipp M (2015) Anatomical Distribution of Cuprizone-Induced Lesions in C57BL6 Mice. J Mol Neurosci 57(2):166–175. https://doi.org/10.1007/s12031-015-0595-5